Shadow Doppler velocimetry with double fiber-array sensors

by

K. Matsuura[(1)] , M. Komaki[(2)] and K. Ueyama[(3)]

KANOMAX Research Institute Co., Ltd.

2-1, Shimizu, Suita, Osaka 565-0805; Japan

[(1)]E-Mail: kazuaki.matsuura@kanomax.co.jp

[(2)]E-Mail: minoru.komaki@kanomax.co.jp

[(3)]E-Mail: koji.ueyama@kanomax.co.jp

ABSTRACT

The shadow Doppler velocimetry (SDV) systems with double fiber-array sensors are developed for the measurements of particle trajectory angles and for the stereoscopic investigation of particles. Their performance is investigated in two application examples; the measurements of particles in oscillating motions and of those in pipe flows. The parallel 2-line fiber-array configuration enables us to measure the trajectory angle in a plane perpendicular to the optical axis, with the measurement errors less than 1.5 degrees. The high accuracy of the present method realizes highly accurate particle shape reconstruction process of shadow signals, compared with that used in the normal SDV with a single fiber-array sensor. The present configuration also provides the information on the other trajectory angle in a plane parallel to that including two laser beams, even though only its absolute value can be obtained. The statistical average of the absolute values of the angles larger than approximately 5 degrees can be measured with the measurement errors less than 3 degrees. In case of stereoscopic measurements where two SDV optical systems are utilized, the shadows of irregularly-shaped particles taken by both optical systems show different particle properties from each other, such as area-equivalent diameters and aspect ratios. This difference is considered to be especially important when the flow characteristics have significant influence on particle orientations. It can be also found by means of the stereoscopic SDV that, in the present pipe flow experiments, the trajectories of particles whose axial velocity is far less than the main flow are influenced by three dimensional effects, possibly derived from the windows installed on the pipe wall.

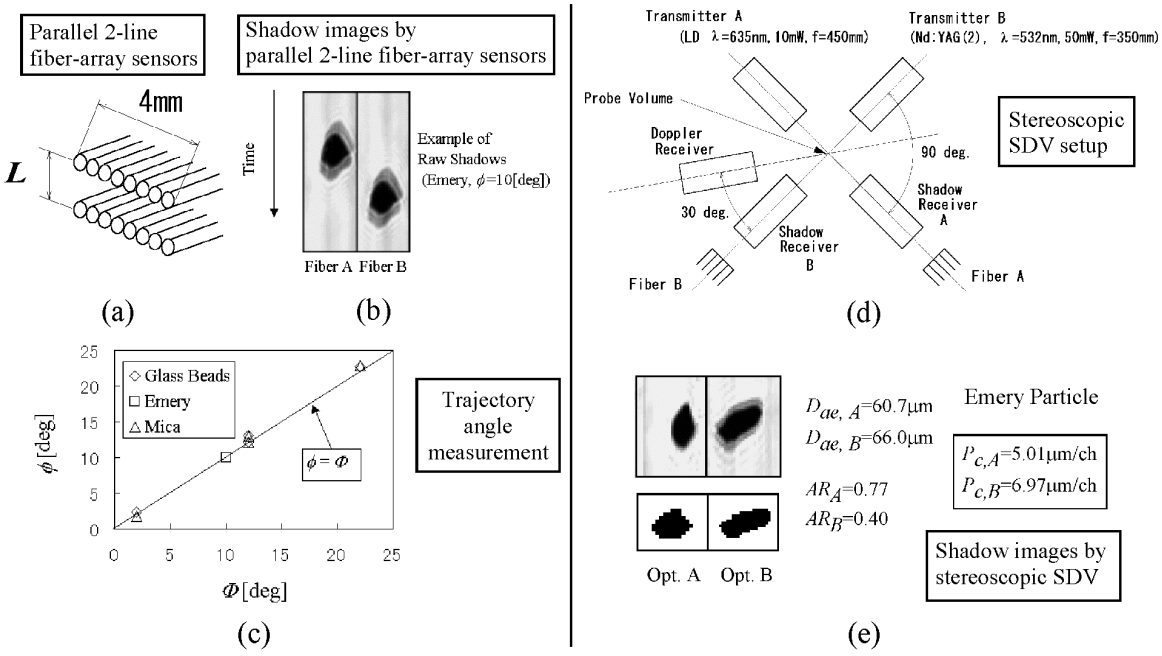

Fig. 1. Shadow Doppler velocimetry with double fiber-array sensors.

1. INTRODUCTION

The shadow Doppler velocimetry (SDV) is a state-of-art measurement technique for multi-phase flows, which realizes simultaneous measurement of particle velocity and size (Hardalupas et al. 1994). Even though some other methods such as the phase Doppler anemometry (Durst and Zaré, 1975) and more recently the novel interferometric laser imaging technique (Maeda et al., 2000) also provide such information, they are only applicable to spherical particles. The most distinctive feature of the SDV is its applicability to arbitrarily-shaped particles, so that so far it has been employed in the research of pulverized coal combustion (Maeda et al., 1997 and Prassas, 1998), paint sprays (Morikita and Taylor, 1998), spray dryers (Hardalupas et al., 2001) and so on. As for instrumental development of the SDV, the first significant improvement was achieved in the work of Hardalupas et al. (1994) and Morikita et al. (1995). Later, the present authors have further improved the system so that the shadow images of particles with their velocity typically up to 100 m/s and their diameter larger than 10 μm can be acquired in 8-bit gray scale levels (Matsuura et al., 2001).

On the other hand, Morikita et al. (1995) also pointed out its ability to measure some extra properties of particles, such as the trajectory angle in a plane perpendicular to the optical axis. The information on the trajectory angle is especially important when precise particle shape reconstruction is required, even though it does not influence the SDV sizing ability itself in principle, as far as area-equivalent diameters are considered. However, the accuracy of the trajectory angle measurement by the normal SDV is not sufficient for particles passing through near the center of the probe volume, with respect to the direction parallel to the optical axis.

In the present study, to improve the measurement accuracy of the trajectory angle, two of 32-channel fiber-array sensors are developed instead of the original 64-channel single fiber-array sensor. Since the total number of the fibers is the same, the other SDV components including the signal processor can be utilized without any further modifications of the normal system. They are installed parallel to each other, whose configuration is similar to that in the research of Kamiwano et al. (1999). Thus, the trajectory angle can be obtained by separation distance between the two fiber-arrays and the displacement of the particle shadows in the direction parallel to them. Furthermore, even though the difference of the view angles (corresponding to the beam-crossing angle) is small, the SDV potentially provides stereoscopic views. Hence, in principle, the present configuration enables us to measure the other trajectory angle in a plane parallel to that including the two laser beams.

In addition, the developed double fiber-array sensors can be utilized for stereoscopic SDV measurement by installing them separately to two independent SDV optical systems. In the research of fluid-particle interaction, the orientation of irregularly-shaped particles in a flow is of great interest. However, for this purpose, the observation of particle shadows from one direction is not sufficient. Hence, the stereoscopic measurement is effective for this kind of applications.

Based on these backgrounds, in the present paper, the basic performance of the shadow Doppler velocimetry systems with double fiber-array sensors mentioned above are examined. For this purpose, two application examples are considered; the first one is the measurement of particles in oscillating motions and the other one is the measurement of particles in pipe flows. The accuracy and advantages of the present techniques will be discussed with the experimental results in later sections.

2. EXPERIMENTAL METHODS

2.1. Basic Principle of Shadow Doppler Velocimetry

The basic principle of shadow Doppler velocimetry is summarized in this subsection. A typical optical set-up of the normal SDV is schematically illustrated in figure 2a. The SDV optics consists of a conventional laser Doppler velocimetry (LDV) and a shadow receiver. The velocity of a particle passing through the probe volume is measured by the LDV. On the other hand, the shadow image of the particle is firstly focused in front of an objective lens, then magnified onto a fiber-array linear image sensor (typically 64 channels), each channel of which is connected to an avalanche photo diode (APD). Therefore, the sensor captures the sliced image of the particle shadow by the two laser beams at each data-sampling moment, which is digitized by 8-bit analog-digital converters for data storage. Finally the particle shape is reconstructed from those sliced images by image-processing with the information of its velocity.

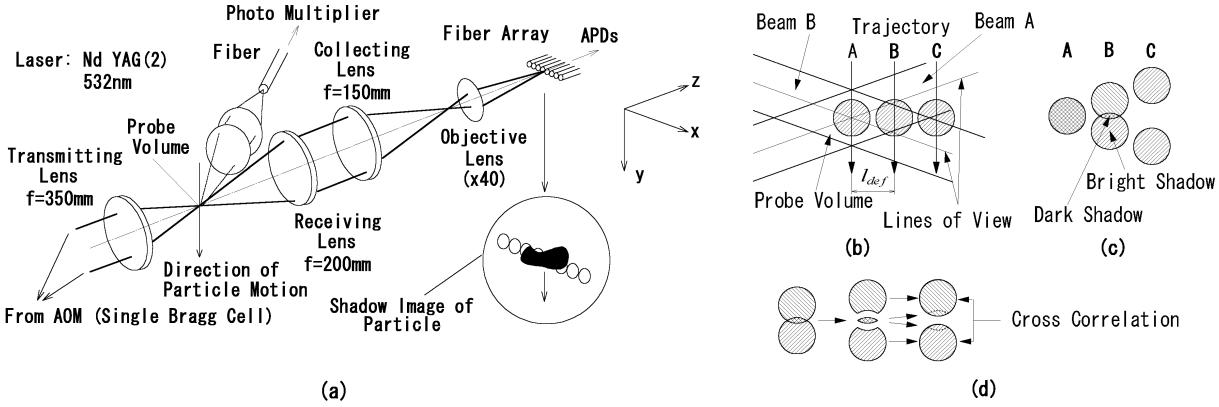

Fig.2. Schematic of optics and principle of Shadow Doppler Velocimetry.

The obtained shadow images can be categorized into three types depending on the "defocus distance (l_{def}) " (Hardalupas et al., 1994) as in figure 2b and 2c, which is the distance in z-direction between the particle trajectory and the right center of the probe volume. In figure 2b, two lines denoted as "lines of view" (more precisely, "planes of view") are view areas of the fiber-array sensor, and it detects a shadow signal when a particle passes across these lines. The acquired shadow images generally consist of a "dark shadow" region where shadows by the two laser beams overlap each other, and "bright shadow" regions where they do not (Trajectory B). They are distinguished by two threshold values so that the shadow by each of two beams is reconstructed as shown in figure 3d. The threshold values are set at 67% and 30% of the light intensity level without shadows (Matsuura et al., 2001). The reliability of the obtained particle shape is examined by taking cross-correlation of the two reconstructed shadows. Note that the area of "dark shadow" region decreases as l_{def} increases. When a particle passes through the right center of the probe volume in z-direction ("in-focus" condition, Trajectory A), the shadows by two laser beams coincide completely. On the other hand, if l_{def} is too large (Trajectory C), the "dark shadow" disappears and such particles are not sampled since the system is triggered only when it detects the "dark shadow".

2.2. Measurement of Trajectory Angle by Parallel Double Fiber-Array Setup

The first application of double fiber-array sensors is the measurement of particle trajectory angles. For this purpose, parallel 2-line sensors are installed instead of the normal single-line fiber-array sensor with 64 channels. Each of them consists of a 32-channel fiber-array. They are placed parallel to each other, with the separation distance L as shown in figure 3a. The similar configuration is also found in the research of Kamiwano et al. (1999), but the present sensors coupled with the SDV system can be applied to the measurements of smaller particles with much faster motions.

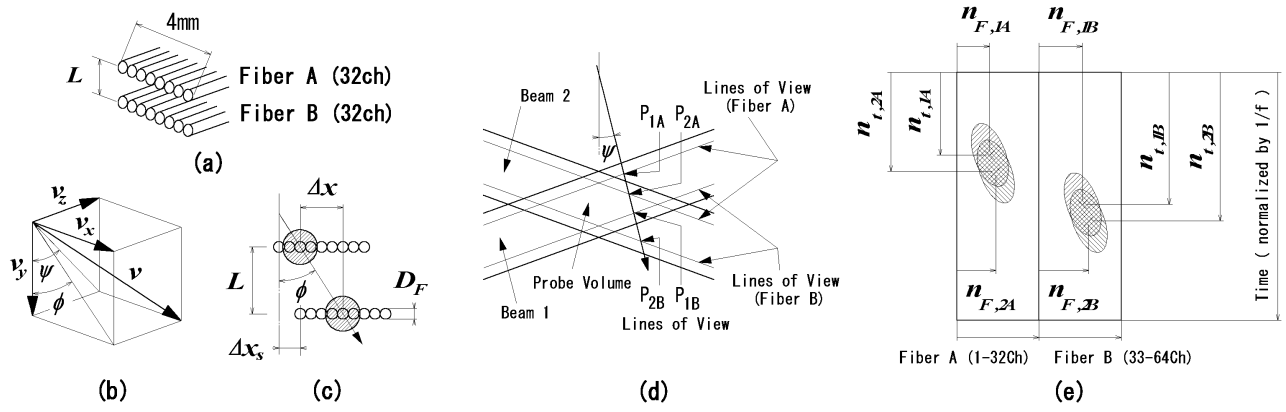

Fig.3. Trajectory angle measurement by parallel 2-line fiber-array sensors.

We at first consider the measurement of the trajectory angle ϕ. It is defined by $\phi = tan^{-1}(v_x/v_y)$ as illustrated in figure 3b, following the same coordinate shown in figure 2a. Here, $\boldsymbol{v}$ is the particle velocity vector and v_x, v_y, and v_z are its

components in x, y and z direction, respectively. There is another trajectory angle $\psi=tan^{-1}(v_z/v_y)$ illustrated in the figure, which is assumed to be zero for the moment and discussed later. The particle shadow motion on the sensor surface is simplified in figure 3c, where D_F and Δx are the fiber diameter and the displacement of the particle shadow in x direction, respectively. From this figure, we obtain $tan\phi = \Delta x / L$. In order to measure large angle of ϕ, the relative position of the sensors in x-direction can be shifted at a distance of Δx_s so that whole particle shadow can be kept within the view areas of the both sensors. For more detailed consideration, the relationship between the particle motion in the probe volume and the schematic of the obtained shadow signals are presented in figure 3d and 3e. For example, when a particle passes across the position P_{1A} at non-dimensional time $n_{t,1A}$, and if the measured non-dimensional x coordinate of P_{1A} (or in other words, the corresponding fiber channel number) is $n_{F,1A}$, the detect the particle shadow by Beam 1 is placed at the position ($n_{F,1A}$, $n_{t,1A}$) in non-dimensional x-t plane as in figure 3e. Here, time is normalized by $1/f$, where f is the sampling frequency of the shadow signal, and x coordinate is normalized by the "pixel coefficient" P_c, which corresponds to the diameter of view area of each fiber. From these figures, we obtain

$$f_\phi \equiv tan\,\phi = \frac{\Delta n_{F,0}}{l_n} \tag{1}$$

where $\Delta n_{F,0} = n_{F,1B} - n_{F,1A} + \Delta n_{F,s} = n_{F,2B} - n_{F,2A} + \Delta n_{F,s}$, $\Delta n_{F,s} = \Delta x_s / D_F$ is the normalized fiber shift by fiber diameter D_F ($D_F = 125\mu m$), and $l_n = L / D_F$ is the normalized fiber separation distance as well. The angle ϕ can be obtained by equation (1). In the present experiments, $\Delta n_{F,0}$ is measured by cross-correlation algorithm. The resolution of the measurement is determined by l_n. The values of l_n chosen for the present experiments are between 8 and 40.

Here, it should be noted that, even in general cases in which ψ is not always zero, equation (1) can be used by only substituting the aforementioned definition of $\Delta n_{F,0}$ with $\Delta n_{F,0} = 2(\Delta n_{F,1}^{-1} + \Delta n_{F,2}^{-1})^{-1}$, where $\Delta n_{F,1} = \Delta n_{F,1B} - \Delta n_{F,1A} + \Delta n_{F,s}$ and $\Delta n_{F,2} = \Delta n_{F,2B} - \Delta n_{F,2A} + \Delta n_{F,s}$, respectively.

On the other hand, the parallel 2-line fiber-array configuration can also provide the information on the other trajectory angle ψ, which was assumed to be zero in the discussion above. In the example of figure 3d and 3e, the normalized time interval $\Delta n_{t,1} = \Delta n_{t,1B} - \Delta n_{t,1A,}$ and $\Delta n_{t,2} = \Delta n_{t,2B} - \Delta n_{t,2A}$ are obtained by $\Delta n_{t,1} = P_c\, l_n\, f\, cos\psi\, cos(\theta/2) / v_y\, cos(\psi - \theta/2)$ and $\Delta n_{t,2} = P_c\, l_n\, f\, cos\psi\, cos(\theta/2) / v_y\, cos(\psi + \theta/2)$, respectively, where θ is the beam-crossing angle (6.6 degrees in the present experiments). By considering the time difference $\Delta n_{t,12} = \Delta n_{t,2} - \Delta n_{t,1}$, we obtain

$$f_\psi \equiv \left| \frac{sin\,2\psi\, sin\,\theta}{cos\,2\psi + cos\,\theta} \right| = \left| \frac{\Delta n_{t,12}}{\Delta n_{t,0}} \right| \tag{2}$$

where

$$\Delta n_{t,0} \equiv \frac{P_c l_n f}{v_y} = 2\left(\Delta n_{t,1}^{-1} + \Delta n_{t,2}^{-1}\right)^{-1} \tag{3}$$

The angle ψ is obtained from equation (2). In the present data processing, $\Delta n_{t,0}$ is obtained by the middle term of equation (3) with v_y measured by the LDV. The values of $\Delta n_{t,1}$ and $\Delta n_{t,2}$ are measured by cross-correlation algorithm. It should be noted that the resolution of the measurement is determined by θ and $\Delta n_{t,0}$, the latter of which is also a function of v_y. The values of $\Delta n_{t,0}$ in the present experiments are in the range between 150 and 420.

In the present ψ measurement, only its absolute value can be obtained due to the symmetry of shadow signals with respect to xy-plane (including the center of the probe volume), as shown in figure 4a. Furthermore, as in the example of figure 4b, in case particle passes across the xy-plane between Q_A and Q_B (Trajectory M), the time order of the shadows by the two laser beams are different between the image taken by Fiber A and that by Fiber B. Therefore, without any information with regard to this order, $\Delta n_{t,1}$ and $\Delta n_{t,2}$ may be wrongly calculated by $\Delta n_{t,1} = \Delta n_{t,1B} - \Delta n_{t,2A}$ and $\Delta n_{t,2} = \Delta n_{t,2B} - \Delta n_{t,1A}$, so that we wrongly obtain ψ_n instead of the correct value, ψ_m.

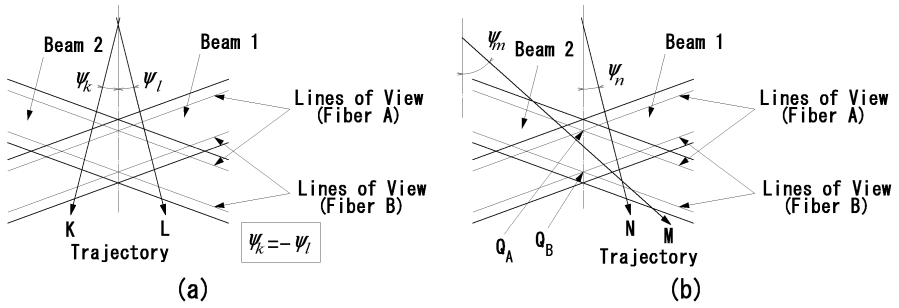

Fig.4. Ambiguity of trajectory angle ψ.

In principle, the order can be assessed by examining if equation (3) is satisfied since $\Delta n_{t,0}$ can be calculated by two different ways (Validation A). Another technique is checking the cross-correlation values, since the wrong order results in less cross-correlation between corresponding pairs of shadow images (Validation B). However, these criteria requires highly accurate measurement of v_y, $\Delta n_{t,1}$, $\Delta n_{t,2}$, and the shadow shapes themselves. In the present paper, a criterion based on the defocus distance is introduced (Validation C), which ensures that the particle trajectory is sufficiently far from the *xy*-plane so that the order is always the same as that shown in figure 3e. If we set the maximal measurable value ψ_{max}, the order is ensured for $\psi < \psi_{max}$ when

$$F_{\psi} \equiv \frac{max\left(\left|\Delta n_{t,A}\right|,\left|\Delta n_{t,B}\right|\right)}{\left|\Delta n_{t,0}\right|} > f_{\psi,max} \tag{4}$$

where $\Delta n_{t,A} = \Delta n_{t,2A} - \Delta n_{t,1A}$, $\Delta n_{t,B} = \Delta n_{t,2B} - \Delta n_{t,1B}$, and $f_{\psi,max}$ is a value of equation (2) when $\psi = \psi_{max}$. In the present study, all the validations above are employed. Since ψ_{max} determines the measurement range and also causes the loss of data with short defocus distance, it should be carefully chosen considering the characteristic of measuring objects.

Finally, typical sensitivity curves of the present techniques for the measurements of ϕ and ψ are presented in figure 5a and 5b, respectively. Even though the angle θ is fixed at 6.6 degrees through all the experiments, the curve for $\theta = 10$ degrees is also presented in figure 5b, to show the effect of θ on the sensitivity.

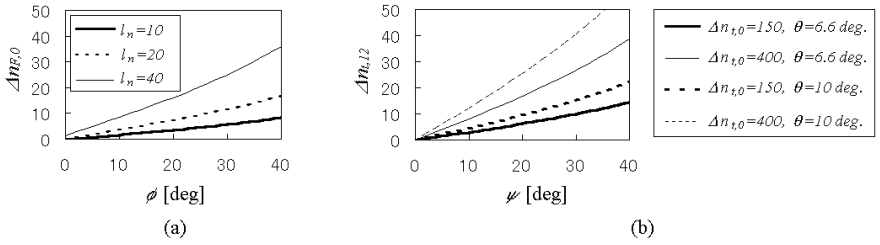

Fig.5. Sensitivity of trajectory angle measurements.

2.3. Stereoscopic Set-Up

The other application of the double fiber-array sensors in the present paper is the stereoscopic measurement. In the research of particle-fluid interaction process, the information on the orientation of particles is required, whose effect is not clarified if we observe particle images from only one-direction. The stereoscopic SDV is effective for such applications. The schematic of stereoscopic SDV optics is illustrated in figure 6. Two SDV optical systems (Optics A: Transmitter A + Shadow Receiver A, and Optics B: Transmitter B + Shadow Receiver B) are installed with the angle between the two optical axes of 90 degrees. The centers of the probe volumes of both systems are carefully adjusted to

coincide each other. Each of the two optical systems is similar to that shown in figure 2, except the transmitters whose specifications are presented in figure 6. As for Doppler signals, only those by the scattering of green light (Transmitter B, λ=*532nm*) are detected in the present experiment. This can be achieved by simply placing the Doppler receiver at the position where it detects the forward scattering signal of the more powerful laser (Transmitter B) so that the side-scattering signal of the less powerful laser (Transmitter A) can be negligible.

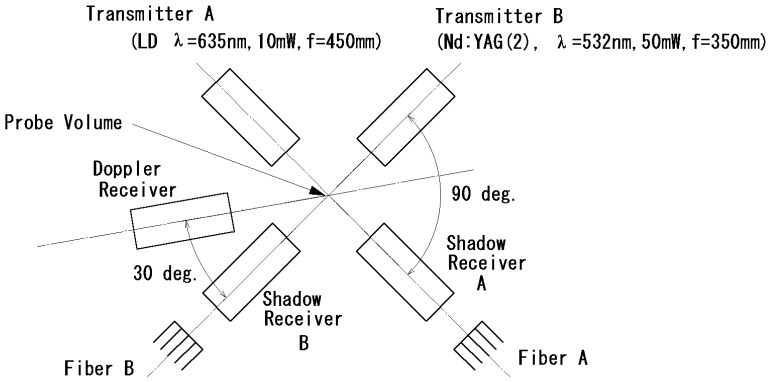

Fig.6. Top view of stereoscopic SDV optics.

2.4. Experimental Instruments

The SDV measurements were conducted by means of a modified system of commercially available SDV (SDPA Model 8250, KANOMAX Japan Inc.). The modification was carried out only with regard to the fiber sensors. Since each of two fiber-array sensors in the present experiments consists of 32 channels, whereas the original sensor has 64 channels, the exactly same signal processing system can be utilized.

To evaluate the performance of the present experimental methods, the following experiments were conducted.

The first experiment (**case A**) is the measurement of circumferentially oscillating particles as illustrated in figure 7a. Either a spherical glass bead or an aluminum particle was used as a test particle, whose area-equivalent diameters (D_{ae}) by microscopic measurements were 63μm and 72μm, respectively. The test particle was fixed between two thin glass plates whose thickness was 0.2mm, and they were fixed at the edge of a disk. The disk was connected to a DC motor, which was driven by a sinusoidally oscillating signal supplied by a frequency generator. This results in a circumferential oscillating motion of the particle, whose velocity was in the range between 0.03m/s and 0.05 m/s. The instrument was equipped with translational and rotational optical stages for the adjustment of the position of the particle with respect to the SDV probe volume and the angles of disk attitude Φ and Ψ as in figure 7a.

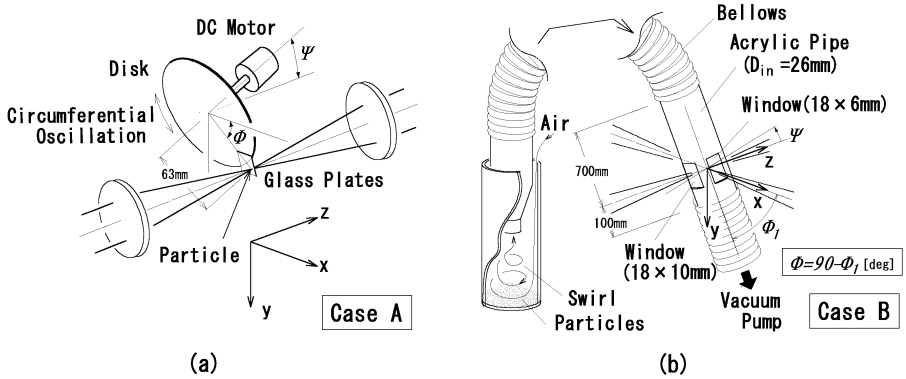

Fig.7. Experimental instruments.

The second experiment (**case B**) is the measurements of particles in pipe flows, which is a more practical application than the aforementioned case. The setup for this experiment is shown in figure 7b. The air flow inside an acrylic pipe

with its inner diameter of 26mm was driven by a vacuum pump downstream. The inlet of the pipe was connected to a particle feeder. The air was introduced from atmosphere through a narrow gap of the particle feeder, and the particles inside the feeder were mixed with the air flow due to the induced swirl motion. Finally, the particles were transported to the test section, which was located 700mm downstream from the inlet of the pipe. The test section was equipped with four thin glass plates as observation windows to avoid unwanted distortion of shadow and Doppler signals. As shown in the figure, the two windows normal to *x* axis and the other two normal to *z* axis were in different shapes. This effect will be discussed with experimental results later. The angles of pipe inclination Φ and Ψ defined as in figure 7b were adjustable. The probe volume was set on the axisymmetric axis of the pipe so that particle velocity vectors should be parallel to the axis if the particles follow the air flow completely and the three dimensional effects caused by the windows are negligible. In the present experiments, the typical mean flow velocity at the test section was in the range between 15m/s and 35m/s, depending on experiments. As test particles, spherical glass beads, emery sands, and mica particles were utilized, whose mean diameters by microscopic measurements were approximately 60μm, 70μm and 40μm, respectively.

It should be noted that the angle Φ and Ψ are defined in a different manner from that of particle trajectory angles ϕ and ψ. However, in the following discussion, we fix either the angle Φ or Ψ as zero so that practically Φ and Ψ can be considered as equal to ϕ and ψ, respectively.

3. RESULTS and DISCUSSION

3.1. Trajectory Angle Measurements of Particle in Oscillating Motions

In the present section, the measurement results of the trajectory angles for **case A** are presented.

Figure 8 shows experimental results for the angle ϕ. For the present experiments, the angle Ψ is fixed at 0 degrees. For large angles more than 25 degrees, the relative position of the sensors in *x*-direction was shifted with $\Delta n_{F,s}$=5. In figure 8a, plotted symbols are experimental data, each of which is the average of approximately 100 samples for the same experimental conditions. They are almost on the solid line, which shows the ideal measurement condition without errors. The measurement errors of the mean values of angle ϕ are less than 1 degree for all the data. On the other hand, the modified standard deviations of ϕ defined as $\sigma_{\phi,m}=(df_\phi/d\phi)\,\sigma_\phi$ are plotted against l_n^{-1} in figure 8b, where σ_ϕ is the measured standard deviation in radian. The solid line in the figure shows $\sigma_{\phi,m}$ derived from 1pixel measurement error of $\Delta n_{F,0}$, which is equal to l_n^{-1} in fact. The experimental data lie far below the solid line, showing that the present method has sufficient accuracy. The standard deviations σ_ϕ without the modification are less than 1 degree in the present case.

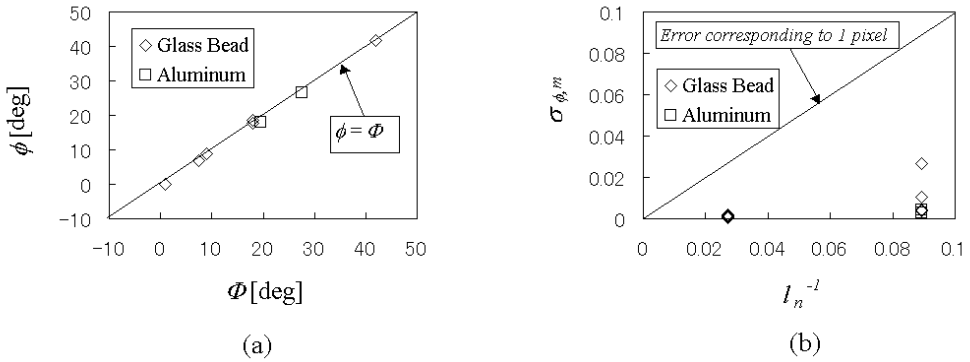

Fig.8. Experimental results of trajectory angle ϕ for **case A**.

Secondly, the results of the other trajectory angle ψ are presented in figure 9. For this experiment, the angle Φ is fixed at 0 degrees. Since the defocus distance is set sufficiently large in the present experiments, the aforementioned trajectory angle ambiguity does not take place. Figure 9a and 9b are plotted in a similar manner to figure 8a and 8b, with the definition of $\sigma_{\psi,m}$ as $\sigma_{\psi,m}=(df_\psi/d\psi)\,\sigma_\psi$, where σ_ψ is the measured standard deviation of ψ in radian. The number of samples for each experiment is also approximately 100. Figure 9a shows good agreement between ψ and Ψ within the errors of 3 degrees but the modified standard deviations $\sigma_{\psi,m}$ are not as small compared with $\sigma_{\psi,m}$ derived by 1pixel

measurement error of $\Delta n_{t,12}$ (solid line), as in figure 8b. Since the measured standard deviations σ_ψ without the modification are less than 1.5 degrees, the performance of the measurement is still good in the present experiment. However, the performance should be examined in the more practical application, whose results will be presented later.

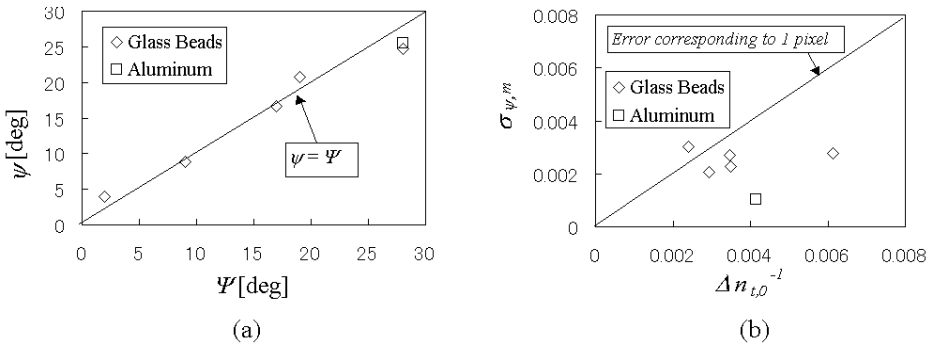

Fig.9. Experimental results of trajectory angle ψ for **case A**.

3.2. Trajectory Angle Measurements of Particles in Pipe flows

The second application example of the present experimental method is on the pipe flow (**case B**).

Figure 10 shows the measurement results of the trajectory angle ϕ. As in **case A**, the angle Ψ is fixed at 0 degrees. An example of raw shadow images and of a histogram of ϕ are presented in figure 10a and 10b. The measurement results of angle ϕ are plotted in figure 10c and 10d in a similar manner to figure 8a and 8b, respectively. The number of samples for each experiment is approximately 1000. Again, the measured angles ϕ show good agreement with Φ within the errors of 1.5 degrees, and the modified standard deviation $\sigma_{\phi,m}$ is less than that derived from 1pixel measurement error of $\Delta n_{F,0}$ (solid line). The standard deviations σ_ϕ without the modification are less than 1 degree, showing that most of particles follow the main flow and the accuracy of the present method is sufficiently high. It is also found from figure 10d that the effect of particle shape is small.

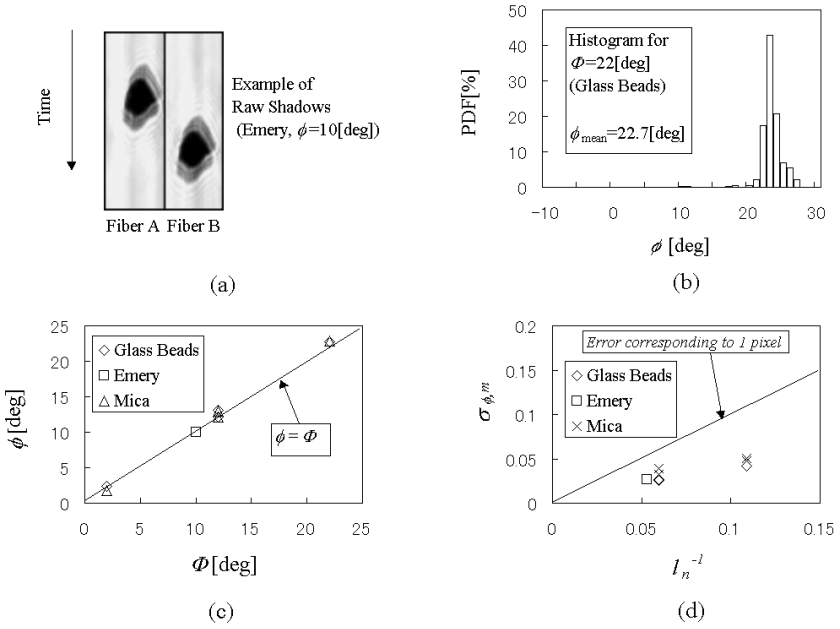

Fig.10. Experimental results of trajectory angle ϕ for **case B**.

As previously mentioned, the normal SDV system can potentially measure the trajectory angle ϕ by the method based on defocused shadow images suggested by Morikita et al. (1995). By the method, the angle can be obtained from the

relationship $tan\ \phi = P_c f \Delta n_{F,A} / v_y \Delta n_{t,A}$, where $\Delta n_{F,A} = n_{F,2A} - n_{F,1A}$. However, its performance is not sufficient especially for the data with small defocus distance. This causes errors in particle shape reconstruction process of the SDV. Figure 11 presents how the performance is improved by utilizing parallel 2-line fiber-array system. In the figure, the measurement accuracy on ϕ and the performance of the reconstruction process are presented for spherical glass beads. To evaluate the reconstruction process, the aspect ration defined by $AR=B/A$ is introduced, where A and B in figure 11c are the length of major and minor axes of particle shadows, respectively, which are assumed to be in elliptic shapes. For comparison, the scatter plot of the aspect ratio without any trajectory angle correction (AR_0) is also presented in figure 11d. As expected, the measurement results by using defocused images (ϕ_{def}) show good performance for large defocus distance, whereas it shows large scatter for small defocus distance. As a result, for small defocus distance, particle shapes which should be spherical are not correctly reconstructed as shown in the figure, resulting in also the scattered data of aspect ratio. On the other hand, the results obtained by the present method ($\phi_{2\text{-}line}$) are independent of defocus distance, and the original spherical particle shapes are successfully reconstructed. This improvement is especially significant in applications where particle shapes and orientations are of great concern.

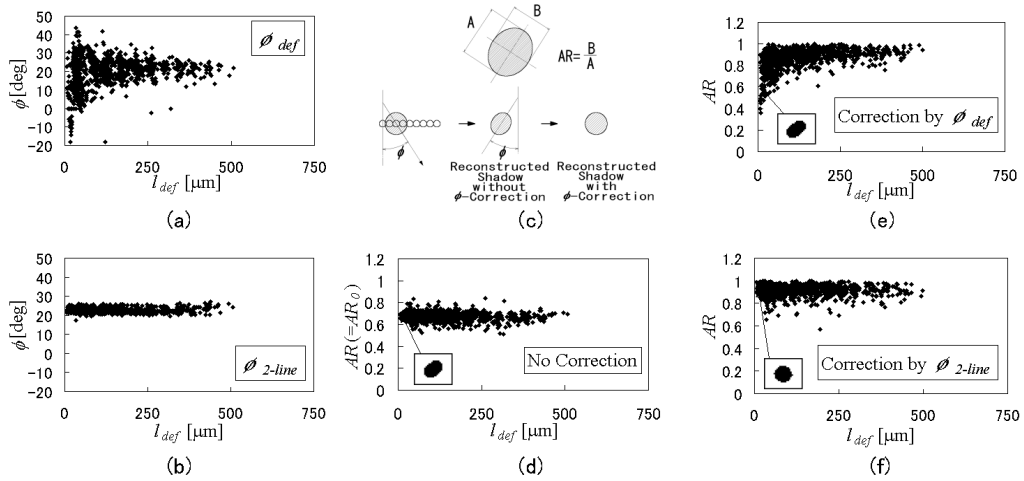

Fig.11. Comparison of performance on trajectory angle and shape measurements between normal SDV and double fiber-array SDV (60μm glass beads, Φ=22 degrees).

With regard to the other trajectory angle ψ, before the evaluation of the data, it is necessary to avoid the aforementioned ambiguity due to the particle trajectory. For this purpose, the performance of the criterion denoted as "Validation C" in the previous section is evaluated. Figure 12 shows an example of this validation process for the data having survived Validation A and B. For example, by setting the maximal measurable angle ψ_{max}=35 degrees, we obtain $f_{\psi,max}$ is 0.081. Thus, only the data satisfying $F_\psi > f_{\psi,max}$ are validated. In figure 12, $f_{\psi,max}$ for ψ_{max} =18 degrees are also presented. The tendency of the correlation between F_ψ and ψ are completely different between the data on the left of this value and those on the right. This shows the fact that the former are wrongly calculated data due to wrongly determined time order of shadow images, whereas most of the latter are correctly calculated so that they are distributed around the correct value of ψ. Hence, F_ψ is an effective index on finding the time order of shadow images, to avoid the ambiguity on ψ.

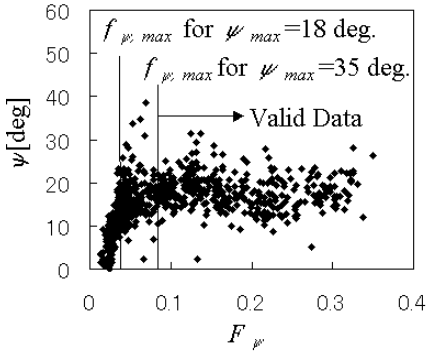

Fig.12. Validation method for ψ measurement based on defocus distance (60μm glass beads , Ψ=18 degrees).

Figure 13 shows the measurement results of particle trajectory angle ψ. As in **case A**, the angle Φ is fixed at 0 degrees. The original data for this figure are validated based on the same criterion as mentioned above with the value of ψ_{max}=35 degrees. An example of raw shadow images and of a histogram of ψ are presented in figure 13a and 13b. The elongated shadow images result from the faster sampling frequency f compared with that in figure 10a, to improve the measurement resolution by increasing $|\Delta n_{t,0}|$. The experimental results of angle ψ are plotted in figure 13c and 13d, in a similar manner to figure 9a and 9b, respectively. The number of samples for each experiment is also approximately 1000. The mean values of the measured angles ψ show good agreement with Ψ within the error of 2 degrees, except the result with a small value of Ψ, which is caused by the fact that only absolute values of ψ can be measured by the present method. On the other hand, the modified standard deviation $\sigma_{\psi,m}$ is larger than that derived from 1pixel measurement error of $\Delta n_{t,12}$. The standard deviations σ_{ψ} without the modification are between 3 and 5 degrees, which are not regarded as small values assuming most of particles follow the mean flow. Considering these values and the relatively large error of mean value for small ψ, the present method should be applied to the angles larger than approximately 5 degrees. Under this condition, the present method for the measurement of ψ is reliable in terms of statistical average. However, further improvement is required for the reliable measurement of ψ for individual particles.

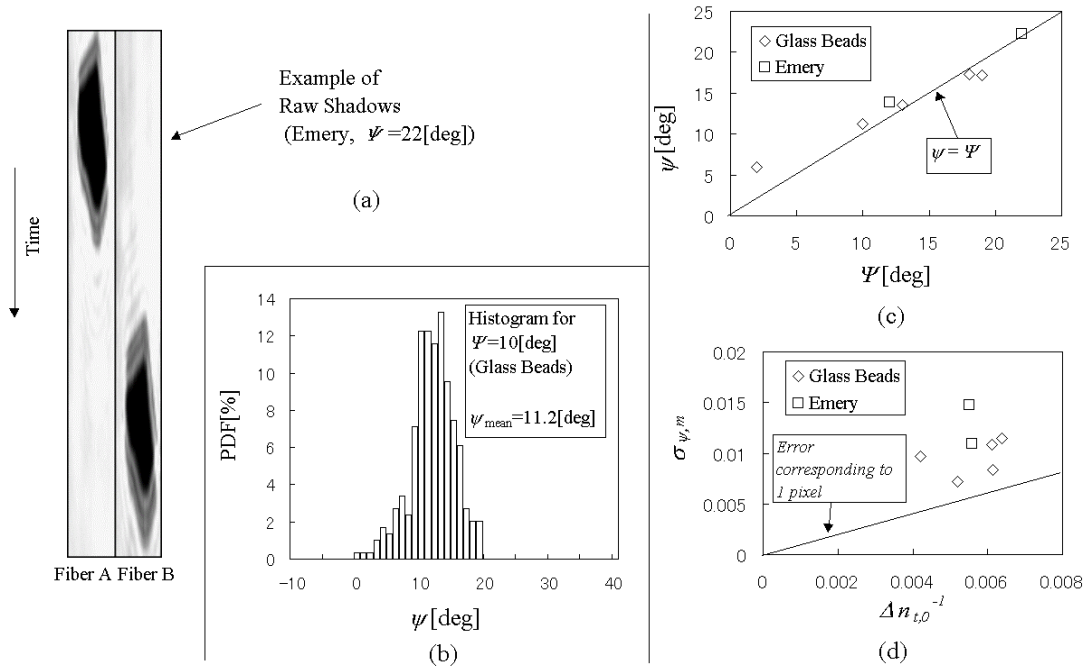

Fig.13. Experimental results of trajectory angle ψ for **case B**.

3.3. Stereoscopic SDV measurements

The results of stereoscopic measurements for **case B** are discussed in this subsection. The angles Φ and Ψ are fixed at 0 degrees. Some examples of raw shadow images and reconstructed shadow images are presented in figure 14.

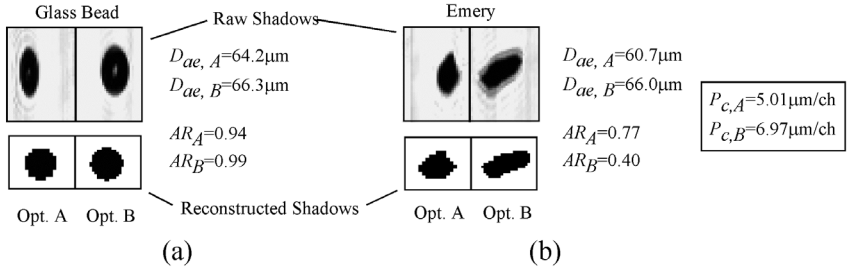

Fig.14. Shadow images obtained by stereoscopic SDV measurements.

It should be noted that pixel coefficients P_c of Optics A and Optics B are different from each other. Shadow signals from both optical systems are almost exactly synchronized, showing the view areas of fiber-array sensors successfully coincide to each other with respect to y-direction. It is obvious that the reconstructed shadows of a spherical glass bead by the results of Optics A and of Optics B are almost identical, whereas those of a non-spherical emery particle show different shapes. It is also true for other particle properties such as area-equivalent diameters D_{ae} and aspect ratios AR as shown in the figure, whose values to be measured are strongly affected by particle orientation if it is not spherical. Thus, the stereoscopic SDV is effective for detailed study of non-spherical particles in a flow.

Experimental results obtained by the stereoscopic SDV can be used in various ways of data analysis. Figure 15 shows one of such examples. Size-velocity correlation of 60μm spherical glass beads in the pipe flow (**case B**) is presented in figure 15a. Most of the particles (Group I) follow the mean flow in the pipe so that their velocity data are distributed within the region between 20m/s and 30m/s in the present case. On the other hand, there are some particles with their velocity far less than 20m/s (Group II). Since their diameters (D_{ae}) are also close to 60μm, this is not due to systematic measurement errors but due to a different physical phenomenon governing their dynamics. To investigate the phenomenon more in detail, the correlation between particle velocity in y-direction (v_y) and its aspect ratio without trajectory correction (AR_0) is plotted in figure 15b. As shown in figure 11c, for spherical particles, deviations of AR_0 from unity is due to the effect of trajectory angle ϕ. In figure 15b, the vertical axis of the upper and the lower figures indicates AR_0 from the results of Optics A and Optics B, respectively. The values of AR_0 for Group I are close to unity in the results of both optical systems. However, most of those for Group II are smaller than those for Group I in case of Optics A, whereas such tendency can not be found in case of Optics B. This can be also observed clearly in figure 15c, where the correlation of AR_0 between both optical systems is presented, with examples of particle shadow images without correction of ϕ . These results imply that the particle motions are influenced by three dimensional effects in case of Group II, but they are not in case of Group I. It is possible that the effects are due to the aforementioned asymmetry of the window shapes, since it may influence on the motions of particles which experience the collision with such an asymmetric inner wall. Even though such discussion is beyond the scope of this paper, it should be emphasized that such investigation becomes possible by introducing stereoscopic SDV measurement, and it would be impossible if the experiments were conducted with only Optics B.

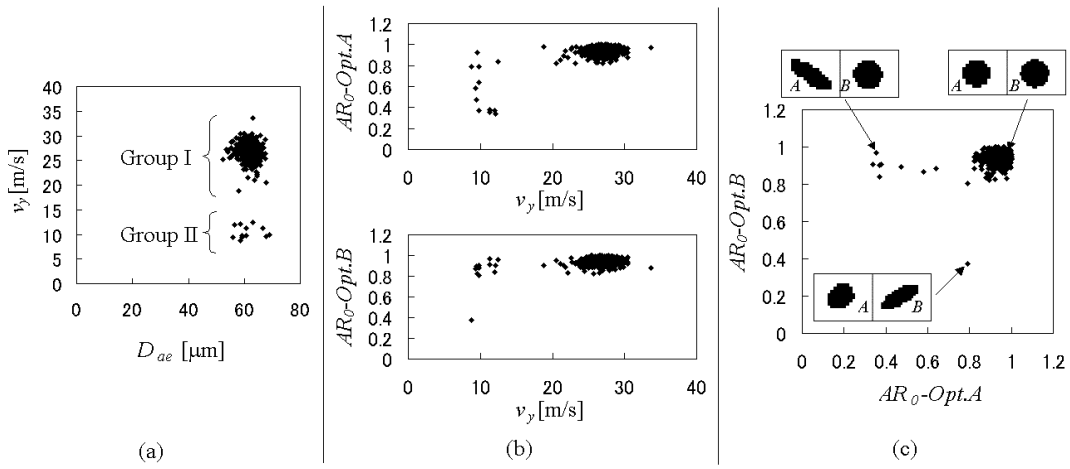

Fig.15. Investigation of two different size-velocity correlation tendency by stereoscopic SDV measurement.

4. SUMMARY

The shadow Doppler velocimetry (SDV) systems with double fiber-array sensors were developed for the measurement of particle trajectory angles and for stereoscopic measurements of particles. Their performance was investigated in two application examples; the measurements of particles in oscillating motions and of particles in pipe flows.

The parallel 2-line fiber-array configuration enables us to measure the trajectory angle in a plane perpendicular to the optical axis. The measurement errors in the present experiments were less than 1.5 degrees, showing high accuracy of the present method. The accuracy was improved compared with that of the normal SDV with a single fiber-array sensor especially for particles passing through near the center of the probe volume with respect to the direction of the optical

axis. This improvement contributed to highly accurate particle shape reconstruction process of shadow signals.

The parallel 2-line fiber-array configuration also provides the information on the other trajectory angle in a plane parallel to that including the two laser beams, even though only absolute values of them can be obtained. The statistical average of the absolute values of the angles larger than approximately 5 degrees could be measured with the measurement errors less than 3 degrees. However, since their standard deviations are 5 degrees at maximum in case of the pipe flow measurements, further improvement is required for the measurements of the angles of individual particles.

In stereoscopic SDV measurements where two SDV optical systems were utilized, examples of particle shadows taken from two different directions in the pipe flow were presented. Since particles in irregular shape show different particle properties such as area-equivalent diameters and aspect ratios depending on view angles, the stereoscopic measurement is considered to be especially important when the flow characteristics have significant influence on particle orientations. In the present pipe flow experiments, some particles did not follow the main flow. It was found that the trajectories of such particles were not statistically axisymmetric, showing the three dimensional effects possibly derived from the windows installed on the pipe wall.

ACKNOWLEDGEMENT

The authors are grateful to Prof. Taylor at Imperial College, Prof. Maeda at Keio University and their research groups for their advice on developing the present shadow Doppler velocimetry system.

REFERENCES

Durst,F. and Zaré, M. (1975). “Laser Doppler Measurements in Two Phase Flows”, Proc. LDA symp., Copenhagen, pp.403-429.

Hardalupas, Y., Hishida, K., Maeda, M., Morikita, H., Taylor, A. M. K. P. and Whitelaw, J. H. (1994). “Shadow Doppler Technique for sizing particles of arbitrary shape”, Applied Optics, 33, (36), pp.8417-8426.

Hardalupas, Y., Kavounides, C., Pergamalis, H., Prassas, I. and Taylor, A.M.K.P. (2001). “Prototype Probe Design and Operating Experience for In Situ Measurements of Particle Size and Velocity in Co-Current Flow Spray Dryer and Spray Dryer Atomisers Using Shadow Doppler Velocimetry”, Spray Drying ’01, Dortmund.

Kamiwano,K., Kaminoyama,M. and Nishi,K. (1999) “The Measurement Method of Dispersed State using Real-Time, High Speed Image Processing System in Multiphase Agitated Vessel”, Proc. 3rd Int. Symp. on Mixing in Industrial Processes, Osaka, pp.211-218.

Maeda, M., Morikita, H., Prassas, I., Taylor, A. M. K. P. and Whitelaw, J. H. (1997). “Shadow Doppler Velocimetry for Simultaneous Size and Velocity Measurements of Irregular Particles in Confined Reacting Flows”, Part. Part. Syst. Charact., 14, pp.79-87.

Maeda, M., Kawaguchi, T. and Hishida, K.(2000).“Novel Interferometric Measurement of Size and Velocity Distributions of Spherical Particles in Fluid Flows”, Meas. Sci. Technol., 11, (12), pp.L13-18.

Matsuura, K., Komaki, M. and Ueyama, K. (2001). “Measurement of Free-Fall Particles by Shadow Doppler Velocimetry”, Proc. 3rd Int. Symp. Measurement Technology for Multiphase Flows, Fukui, Japan, pp.112-120.

Morikita, H., Hishida, K. and Maeda, M. (1995). “Measurement of Size and Velocity of Arbitrarily Shaped Particles by LDA Based Shadow Image Technique”, Developments in Laser Techniques and Applications to Fluid Mechanics, Springer-Verlag, pp.354-375.

Morikita, H. and Taylor, A. M. K. P. (1998). “Application of Shadow Doppler Velocimetry to Paint Spray: Potential and Limitations in Sizing Optically Inhomogeneous Droplets”, Meas. Sci. Technol., 9, (2), pp. 221-231.

Prassas, I. (1998). “Combustion of pulverised coal in swirl burners”, Ph.D. Thesis, University of London.